JOURNAL OF THERMOPHYSICS AND HEAT TRANSFER
Vol. 7, No. 4, Oct.–Dec. 1993

Flow and Heat Transfer in Simulated Re-Entry Vehicle Tile Gaps

Suresh V. Garimella*
University of Wisconsin at Milwaukee, Milwaukee, Wisconsin 53201
Kim A. Shollenberger† and Pamela A. Eibeck‡
University of California at Berkeley, Berkeley, California 94720
and
Susan White§
NASA Ames Research Center, Moffett Field, California 94035

Experiments were performed to investigate the flow patterns and convective heat transfer characteristics in intersecting tile gaps on space vehicles. The flow in a water channel simulates the external flow, and gaps with a depth to width ratio of 20 are mounted as recesses in the bottom wall. A "parallel" gap is installed at 18 deg to the flow direction and ends in a perpendicular gap normal to the flow direction. Gap flow patterns and temperature distributions are obtained as functions of the gap-width-based Reynolds number, the relative height between tiles at the T intersection, and the temperature difference between gap and external flows, using dye entrainment, liquid crystals, and a grid of surface thermocouples. External flow penetration into the perpendicular gap was limited to roughly two gap widths while greater entrainment occurred in the parallel gap. The 18-deg angle of the parallel gap led to asymmetries about the centerline in the perpendicular gap flow patterns and convection coefficients. Natural convection was the predominant mode of heat transfer in the bulk of the perpendicular gap. The Reynolds number and relative tile-height differences had the strongest influence on heat transfer and affected both the magnitude and the asymmetry of the temperature and flowfields.

Nomenclature

D_h = channel hydraulic diameter
H_s = nondimensional step height, h_s/W
h = heat transfer coefficient
h_s = height of step for rear tile
k = thermal conductivity
Nu = Nusselt number, hW/k
Re = Reynolds number, UW/ν
T_c = average temperature of coolant
T_s = gap surface temperature (on heat exchanger)
T_∞ = channel water temperature
U = mean channel velocity
W = width of tile gap
X = nondimensional x, x/W
x = horizontal (spanwise) coordinate along perpendicular gap
Y = nondimensional y, y/W
y = vertical coordinate along perpendicular gap
θ = nondimensional temperature, $(T_s - T_c)/(T_\infty - T_c)$
ν = kinematic viscosity

Introduction

THERMAL protection of space vehicles is accomplished by means of an exterior layer of refractory tiles. Adequate gaps are provided between tiles to allow for thermal expansion. During atmospheric re-entry, high-speed air from the boundary layer of the vehicle enters the gaps. Under severe conditions, hot air can get trapped in the tile gaps and cause overheating of the tile material. When these conditions are anticipated on the basis of empirical predictions, the gaps can be filled with flexible material in order to prevent the hot surface air from flowing into, and stagnating in, the gaps. Modeling efforts have been in progress to predict the flow and heating in the gaps between tiles on the space shuttle. However, fundamental flowfield information is required to develop accurate models that will predict heat transfer rates at gap intersections and under various external boundary conditions.

Space Shuttle tile gaps are typically 0.13-cm wide, 15-cm long, and 2.5- to 15-cm deep. Both ends of the gap are closed such that the gap forms a long, narrow cavity with an open top. The external boundary layer that passes over the gap drives the flow within the gap. The typical external boundary-layer Reynolds number based on development length is 6000, leading to gap Reynolds numbers on the order of 1–10.

Previous numerical models[1,2] have assumed that flow in the tile gaps is two-dimensional, with the flow direction limited to the u and w components of velocity (i.e., flow along the depth and length of the gap, respectively). These models do not consider three-dimensionalities in the flow caused by complex geometries, such as the intersection of one gap with a perpendicular gap. Before the numerical models can be modified to solve for three-dimensional, unsteady gap flows, these flow features need to be documented experimentally. A number of boundary conditions such as the external flow Reynolds number can be expected to strongly affect flow within the tile gaps. The laminar or turbulent nature of the external flow could govern the unsteadiness induced in the gaps. Previous studies with parallel ribs and rectangular cavities (for instance, Neary and Stephanoff[3]) have shown that vortices induced in gap flows are oscillatory in nature.

The flow at the T intersection between perpendicular tile gaps has not been previously studied. However, several studies in the literature have investigated lid-driven cavity flow which bears a resemblance to the present problem, with one important difference. Lid-driven cavity flows have a known driving velocity imposed at the top of the gap using devices such as constant-speed belts. In the present study, on the other

Received March 3, 1992; revision received Dec. 15, 1992; accepted for publication Dec. 15, 1992.

*Assistant Professor, Department of Mechanical Engineering.
†Research Assistant.
‡Associate Professor, Department of Mechanical Engineering.
§Research Scientist. Member AIAA.

hand, the velocity (U) appearing in the Reynolds number is merely the external flow velocity; the actual velocity at the top of the gap could be much smaller than U, due to the effect of the external boundary layer. The present flow would thus be better characterized as shear-driven.

Steady flow within rectangular cavities perpendicular to the flowfield was investigated analytically and experimentally by Pan and Acrivos.[4] The gap aspect ratio (depth-to-width) ranged from 0.25 to 10, and the Reynolds number (UW/ν) range was 20–4000. At low Reynolds numbers ($Re < 400$), inertial forces were neglected and a similarity solution was used to solve for the flowfield. The primary vortex remained unaffected by the depth of the gap for aspect ratios greater than 2. Additional vortices with alternating circulation were formed beneath the primary vortex for the deeper cavities; as the gap was traversed downwards, vortex size decreased slowly while vortex strength decreased rapidly. The size of the primary vortex was 1.4 gap widths for aspect ratios greater than 2. For infinite cavities (aspect ratio of 10), the primary vortex was found to grow with Reynolds number for $Re > 800$, with its size becoming proportional to $Re^{0.5}$ in the range $1500 < Re < 4000$.

Rhee et al.[5] studied a similar configuration, but with an added temperature gradient imposed by cooling the cavity at the bottom. The aspect ratio of the gap was one, and the Reynolds number range 1000–35,000. Liquid crystals suspended in water were used to visualize the flow patterns in the cavity. It was found that the time-averaged equilibrium flow structure in the thermally stratified case was characterized by several additional circulation cells in the cavity, relative to the isothermal case. A synthesis of qualitative and quantitative results describing the flow in this thermally stratified lid-driven cavity flow with unity aspect ratio is presented in Koseff and Street.[6] The flow was shown to be strongly three-dimensional, and turned unsteady at higher Reynolds numbers.

A large body of literature has dealt with flow over a backward-facing step. Many of these studies (for instance, Jaroch and Fernholz[7]) have shown that even in nominally two-dimensional flows over rib-like obstacles, three-dimensionalities are significant and cannot be neglected.

The motivation for the present study was to provide experimental underpinnings for the numerical modeling effort underway at NASA for thermal control of the Aeroassist Flight Experiment (AFE) vehicle. The unique shape of this vehicle renders the perpendicular tile gaps to be at a 72-deg angle. One such tile-gap intersection is modeled experimentally in the present study. In this simulation, the gap width and depth are scaled up by a factor of 5 in order to obtain detailed flow information; the ratio of width-to-depth, however, is matched with the actual conditions. The working fluid is water which has a kinematic viscosity roughly five times that of air.

The objective of this investigation was to gain a qualitative understanding of the flow patterns within narrow gaps under different geometric and external boundary-layer flow conditions. The parameters of study were the external flow Reynolds number (UD_h/ν), the relative height between tiles at a T intersection, and the temperature difference between gap and external flow. The experiments included flow visualization to study the flow patterns, as well as the use of liquid crystals and surface thermocouples to determine the temperature distribution within the gaps. A three-dimensional finite element analysis was performed on the gap walls to obtain surface temperature gradients and heat transfer coefficients.

Experimental Setup and Procedures

An open-loop, constant-head water channel was used for the experiments. A schematic of the flow loop is shown in Fig. 1. Details of operation of the flow facility are provided in Garimella and Eibeck.[8] The channel is rectangular (36.6-cm wide by 4.2-cm high by 180-cm long) with an aspect ratio of roughly 9 to 1, and is made of Plexiglas® for optical access. Careful flow conditioning upstream of the test section ensures uniform flow across the channel cross section.

The intersecting gaps were incorporated into a hatch that forms the bottom wall of the test section, as shown in Fig. 2. The cavities are simulated by Plexiglas enclosures as shown. The T intersection studied is between so-called parallel and perpendicular gaps. The parallel gap is oriented at an angle of 18 deg to the channel flow direction and ends in a perpendicular gap that is at right angles to the flow direction. The gaps are 0.635-cm (0.25-in.) wide and 12.7-cm (5-in.) deep. The aspect ratio of these gaps is identical to the actual tile gaps which are 0.127-cm wide and 2.54-cm deep. The spanwise extent of the perpendicular gap is 25.9 cm while the length of the parallel gap is 40 cm. The end-wall effects for both gaps should be negligible according to Koseff and Street.[9] A stainless-steel heat exchanger installed in each gap provides the requisite temperature differences between external boundary-layer flow and gap flow. Coolant is circulated through passages milled in the heat exchangers which form one wall of each gap; the opposite Plexiglas wall of each gap provides visual access.

The intersecting-gap configuration thus obtained differs from the actual tile gaps in that only one side of each simulated gap is heated. Though this changes the boundary condition, this arrangement of heat exchangers was necessary for providing visual access. Moreover, the more significant requirement of establishing a temperature difference between the gap and channel flows is satisfied. Results presented in this article must be understood in the light of this difference between the simulated and actual situations.

Flow visualization was accomplished by entraining sheets of dye (neutrally buoyant methylene-blue solution) into the channel flow from dye slots as shown in Fig. 1. Dye flow patterns were recorded on a video camera. Temperatures on the gap wall were visualized using liquid crystals. A cholesteric

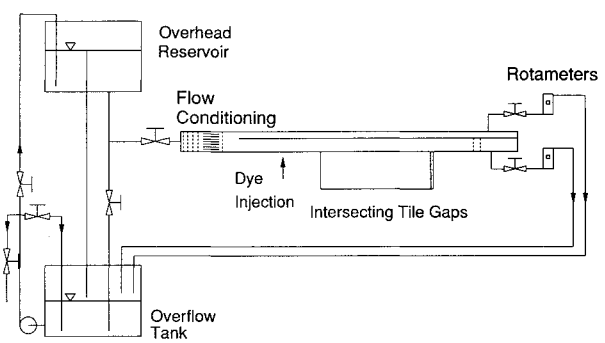

Fig. 1 Schematic of the test facility.

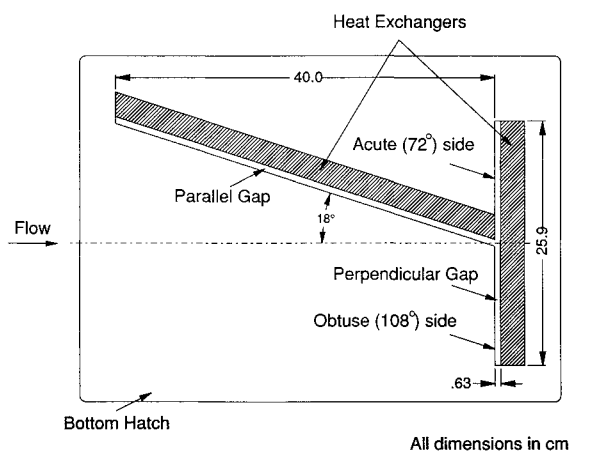

Fig. 2 Plan view of the intersecting tile gaps recessed into the bottom hatch (visual access to gaps in frontal view).

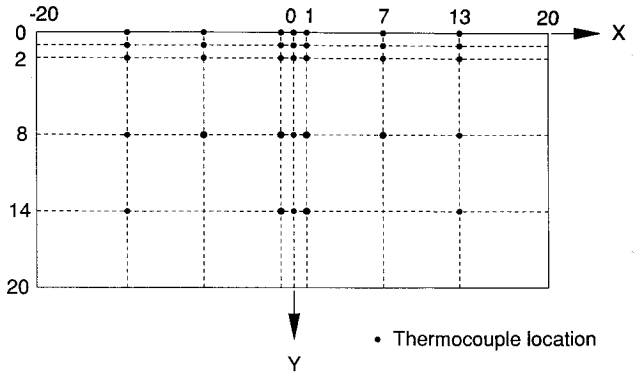

Fig. 3 Thermocouple locations on the perpendicular gap heat exchanger.

liquid-crystal solution with event temperatures ranging from 12 to 13°C was used. Temperature measurements were also made using thermocouples epoxied to the heat exchanger surface. Thirty-three thermocouples (T type, 30 gauge) were used to obtain gap wall temperatures at locations as shown in Fig. 3. The uncertainty in temperature measurement using these thermocouples was determined to be approximately ±0.5°C. Inlet and outlet fluid temperatures in the channel and heat exchangers were also measured using thermocouples. All thermocouples were directly monitored using a Fluke Helios I computer front end hooked up to an IBM PS/2 computer.

The experiments were conducted at four channel flow rates with gap Reynolds numbers (UW/ν) of 90, 145, 200, and 290, and for heat exchanger coolant temperatures of 0, 5, and 10°C, at a nominal freestream temperature of 25°C. Tests were also run at zero flow rate. To study the influence of height differences between tiles at the T intersection, the height of the perpendicular tile was increased by 0, 0.5, 0.75, and 1 gap widths. This was accomplished by attaching appropriate shims on the downstream wall of the perpendicular gap, on top of the heat exchanger (see Fig. 2). Temperature readings were recorded once every 10 s and averaged over a 10-min period, after first allowing approximately 1 h for the system to reach steady state.

A three-dimensional finite element program was developed to analyze the temperature data and calculate heat transfer coefficients. The three-dimensional steady-state conduction equation was solved in the perpendicular heat exchanger with global conservation of energy. Local heat fluxes at the surface of the heat exchanger, which forms the wall of the perpendicular gap, were calculated. These were then used to calculate convection coefficients with the channel exit temperature as reference.

A finite element approach was necessary in order to handle the complex geometry of the heat exchanger as well as the irregular mesh of surface thermocouple locations shown in Fig. 3. The measured temperatures at these locations supplied the boundary conditions for the two active sides (top and front face) of the heat exchanger. Measurements of the heat-exchanger coolant temperature were used for the third surface (back face). The remaining three sides in contact with the Plexiglas encasement were assumed to be perfectly insulated. Other details of the finite element calculations are provided in Shollenberger.[10] The accuracy of the code was checked by verifying the results with a two-dimensional calculation for which a closed-form analytical solution was available.

Results and Discussion

The flow visualization and heat transfer results from this study shed light on the major features of the flow within tile gaps. Flow visualization results are presented first, followed by heat transfer results obtained using liquid crystals and thermocouples.

Flow Patterns

A synthesis of the observations from the flow visualizations using dye entrainment is presented here. Some portion of the main channel flow is entrained into the parallel gap for all flow rates. Even when the channel flow is turbulent, the flow appears to relaminarize after penetrating roughly two gap widths (W) into the gap, and proceeds towards the perpendicular gap. On reaching the intersection with the perpendicular gap, the flow turns preferentially into the obtuse (108-deg-angle) side of the perpendicular gap, eventually flowing upward towards the top of the gap. The bottom corner of the obtuse side of the perpendicular gap remained free of dye for all flow rates tested. Closer to the centerline of the gap, however, in a region half the gap width in each direction, the parallel flow penetrates the perpendicular gap along the entire depth, with the impingement velocity ranging from zero at the bottom to the channel velocity at the top.

The perpendicular gap has two interacting flow components. The channel (external) flow penetrates this gap, forming a primary vortex roughly $1.5W$ deep. The entrained flow from the parallel gap pushes this vortex out into the main flow every 2–5 s, thus leading to a periodicity in the vortex formation. The primary vortex in the acute (72-deg angle) side of the perpendicular gap is stable in contrast, since the parallel gap flow does not effectively penetrate this side of the perpendicular gap. The primary vortex size of $1.5W$ agrees surprisingly well with the value of $1.4W$ obtained by Pan and Acrivos[4] for gap aspect ratios greater than 2.

The addition of a step of height $1W$ to the top of the perpendicular gap heat exchanger results in the primary vortex increasing in size from 1.5 to $2.5W$. In addition, the channel flow penetrates this gap to an increased depth of 3–4 gap widths as shown by the presence of dye at a greater depth. Addition of the step does not noticeably change the parallel-gap flow patterns.

Heat Transfer

A qualitative description of the temperature field was first obtained using liquid crystals. The event temperatures of the liquid crystals used were in the range of 12–13°C, with colors going from black to red to green to blue and back to black again as the temperature increases. The coolant temperature for liquid crystal observations was therefore set to 10°C; at this temperature, the most widespread color changes were observed on the parallel and perpendicular heat exchangers. From all the liquid-crystal photographs obtained, a schematic is derived for the temperature field in the gaps as shown in Fig. 4. The photographs on which this schematic is based are available in Ref. 12.

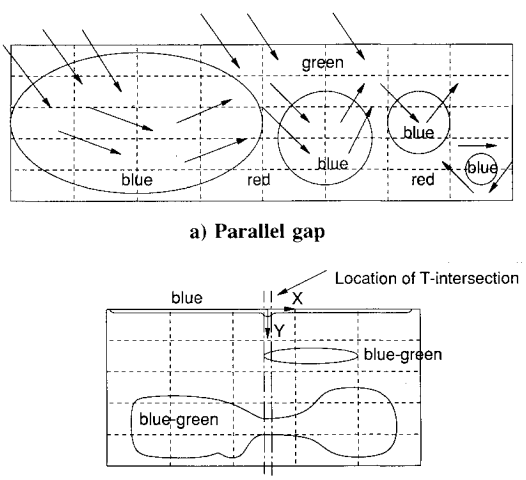

Fig. 4 Schematic of the observed temperature field and flow patterns.

Four circulation zones (blue regions) were visible in the parallel gap. Other circulation regions that must be present to satisfy the sense of the four patterns shown were not visually observed and are not included. A higher-resolution technique of visualization would be required to identify all the zones. The fluid that enters the gap at the upstream end is eventually reflected back into the main flow by the gap floor, as shown by the arrows in Fig. 4a, which are based on the behavior of dye streaks entrained into the flow. This upward flow interacts with that entering the gap further downstream and gives rise to the observed patterns. Several low-velocity regions form in the parallel gap due to these interactions, and are seen as red areas on the liquid-crystal-coated wall. Temperatures in these regions are thus proportionately lower. The parallel gap flow eventually collides with the perpendicular gap and forms the recirculation zone shown in the bottom right of Fig. 4a.

The perpendicular gap is, in general, cooler than the parallel gap, signifying the relatively smaller extent of penetration by the warmer channel flow. A narrow blue region roughly half a gap width in depth was formed at the top of the perpendicular gap where the fluid is warmest, becoming cooler approximately 1–2 gap widths down into the gap. Other warm regions in this gap are outlined in Fig. 4b. The effect of the slanted nature of the parallel gap is clearly visible in the asymmetry of the temperature field in the perpendicular gap. Addition of a step of height $0.75W$ leads to an enhancement in the size and brightness of colors representing the warm regions in the central part of the gap. In addition, the blue (warm) bands at the top of the gap now extend an additional gap width further into the gap due to the addition of the step, for all Reynolds numbers.

Quantitative information about the gap heat transfer was obtained from the surface thermocouples mounted on the perpendicular-gap heat exchanger. The choice of thermocouple location was based on the information obtained from the liquid crystals: thermocouples were concentrated at the region of intersection of the parallel and perpendicular gaps, and towards the top of the perpendicular gap heat exchanger, as shown in Fig. 3. Results are presented in terms of a nondimensional temperature, $\theta = (T_s - T_c)/(T_\infty - T_c)$. The value of θ ranges from 0 to 1 and is proportional to the surface temperature. Space coordinates and length dimensions are nondimensionalized against W, which is also the length scale in Reynolds (UW/ν) and Nusselt (hW/k) numbers. The temperature difference used in calculating the heat transfer coefficient is $(T_\infty - T_s)$. A detailed error analysis revealed uncertainties of ± 0.05 in θ values and ± 2.0 in calculated Nusselt numbers.

Baseline Case

Test conditions with a gap Reynolds number of 90, a coolant temperature of 0°C, and with no difference in height between tiles are designated the baseline case. Subsequently, results will be presented that highlight the influence of the three parameters of this study (coolant temperature, Reynolds number, and relative tile height) on the gap flow heat transfer.

The variations of θ and Nu with horizontal and vertical locations in the perpendicular gap are illustrated in Fig. 5. Three important features of the perpendicular gap heat transfer can be observed from this figure:

1) The temperature and heat transfer coefficient are horizontally stratified and increase sharply towards the top ($Y = 0$) as the gap is traversed upwards.

2) The θ and Nu profiles are not symmetric around the centerline ($X = 0$) of the perpendicular gap.

3) There are significant local variations of θ and Nu about the centerline, in the region $-1 \le X \le 1$, and markedly so for $Y < 2$.

The origin of the asymmetries appears to be primarily due to the presence and orientation of the parallel gap. The fluid that is cooled while traversing the parallel gap causes a suppression of temperature where it impinges onto the perpendicular gap. This fluid is then projected into the obtuse side of the perpendicular gap due to the 108-deg angle ($X < 0$), and enhances mixing in this part of the gap. The close proximity of the cold heat exchanger in the parallel gap to the centerline of the perpendicular gap also contributes to this local suppression of temperature.

It is clear from Fig. 5 that for $Y \ge 8$, θ takes values of 0.02, which indicates that the temperature in these lower locations of the gap is almost identical to the coolant temperature. The Nusselt number in this region also lies in the 0–1 range, indicating the absence of forced convection. Natural convection and conduction are thus the significant modes of heat transfer in this region. This is further evidence of the observation from flow visualization that the penetration of bulk fluid at the Reynolds numbers of this study is limited to a few gap widths.

For the higher locations in the gap, $Y = 1$ and 2, a noticeable increase in θ occurs. However, Nu increases only for $Y = 1$. This leads to the conclusion that the increase in θ at $Y = 2$ is a consequence of conduction along the gap (heat exchanger) surface, and not due to an increase in convection. At $Y = 1$, however, since θ and Nu both increase, it is reasonable to assume that enhanced convection is the cause. The parallel gap-flow induced asymmetries near the centerline also become pronounced at these y locations.

The values of θ and Nu are much greater at the top of the perpendicular gap than at any depth, as seen from the graph for $Y = 0$. The greatest variations near the centerline also occur at $Y = 0$ where direct impingement of the cooled parallel gap flow causes a significant suppression of θ and Nu, especially at $X = 1$. As the gap is traversed away from the centerline in either direction, θ and Nu increase (after an initial dip), implying greater convective heat transfer rates. The dips in θ and Nu on either side of the centerline result from the complex interactions of the impinging parallel gap flow with the entrained channel flow and are difficult to explain.

Having examined the general features of the baseline case, results are now presented that illustrate the influence of three system variables on convective heat transfer in the gaps.

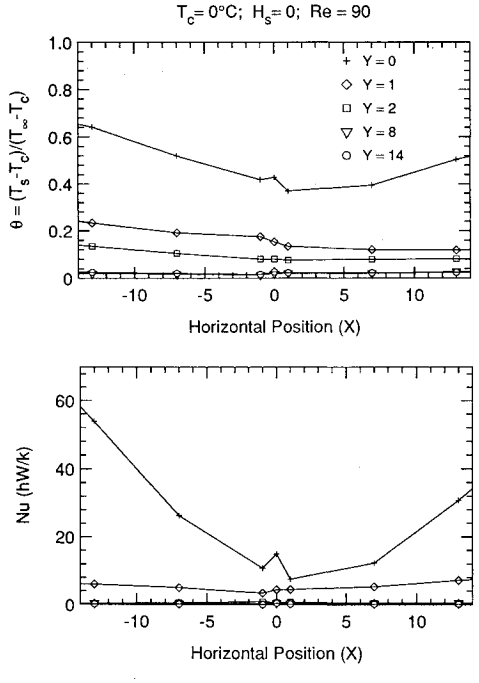

Fig. 5 Temperature and Nusselt number distribution in the perpendicular gap for the baseline case.

Effect of Coolant Temperature

Surface temperature results were obtained for three coolant temperatures, T_c = 0, 5, and 10°C, for Re = 90, 145, 200, and 290. The purpose of studying this parameter was to determine its effect on the forced and free convection heat transfer rates, as well as to verify the accuracy of the experimental technique. The results showed that there was no discernible effect of coolant temperature at all Reynolds numbers and for all spatial locations. In view of this, the temperatures obtained with the three different coolant temperatures were used to estimate overall experimental uncertainties. The average standard deviation in measured θ (averaged over 132 cases: at 4 Reynolds numbers, 3 coolant temperatures, and at 33 thermocouple locations) was found to be 0.01. Based on this independence of θ (and Nu) on T_c, the results presented in this article are averaged values over all coolant temperatures.

Effect of Reynolds Number

Experiments were performed at four channel flow rates spanning both flow regimes in the channel (external flow), with gap Reynolds numbers of 90 (laminar), 145 and 200 (transitional), and 290 (turbulent). Natural convection results obtained with zero flow (Re = 0) are also presented in these figures but are discussed in a later section. The variation of θ and Nu with Reynolds number is depicted in Figs. 6 and 7, respectively. The figures show data at four Y locations (Y = 0, 1, 2, and 8), and are plotted to different scales. As Reynolds number increases, it is clear that both θ and Nu increase in all the plots, especially for $0 \le Y \le 2$. The increases in θ and Nu with Re are greatest at the top of the gap, Y = 0, while at Y = 8 and 14, changes with Re are almost negligible (note the change in scale). The influence of Re therefore appears limited to roughly 1–2 gap widths.

Both θ and Nu are influenced by the asymmetry of the flow around the centerline of the perpendicular gap. The effect of the impinging parallel gap flow is quite pronounced in the region around the centerline. At Y = 0, 1, and 2, the shape of the θ vs X graph changes as Re increases. The rise in θ with Re is much sharper at X = 0 and 1 than at X = −1. The peak at the centerline shifts from X = 0 to X = 1 at the higher Reynolds numbers of 200 and 290. The same trends of variation are also found true for Nu. The small differences in the behavior of θ and Nu are attributable to the smearing of temperatures at Y = 1 and 2, due to conduction in the perpendicular heat exchanger. The increased flow towards the obtuse side of the perpendicular gap also affects θ and Nu values at $X > +1$. The contrast between values in the $+X$ and $-X$ portions of Figs. 6 and 7 illustrates this well. Increasing the Reynolds number thus appears to increase entrainment in the parallel gap, leading to greater impingement of cooled flow into the perpendicular gap. The direct entrainment of channel flow also increases.

One other feature of the dependence of temperatures on Reynolds number is of interest. The standard deviation of temperatures (T_s) averaged over X at Y = 0 (the top of the perpendicular gap) rose sharply from 0.03 to 0.79°C as the Reynolds number was increased from 90 to 200, and leveled off at 0.87°C at Re = 290. At a depth of one gap width (Y = 1), the corresponding increase in standard deviation of T_s was from 0.02 to 0.39°C. No changes in standard deviation with Reynolds number were noticed for $Y \ge 2$. These results may either reflect a transition in flow regimes or an increase in the frequency at which the primary vortex formed in the perpendicular gap is ejected into the external flow. The region of direct influence of the channel flow appears to be limited to a depth of about 1–2W into the gap. It is to be noted, however, that the thermocouple readings were recorded only once every 10 s. The standard deviations listed here should thus not be taken to be any direct measure of turbulence levels.

Effect of Tile-Height Differences

The influence on the gap flow heat transfer of increasing the height of the perpendicular tile with respect to the parallel tiles is presented next. The step heights (h_s) investigated were 0, 0.5, 0.75, and 1.0 gap widths. Figures 8 and 9 depict the variation in θ and Nu as the relative tile height is changed. At the top of the gap (Y = 0), there is little effect of changing the step height on θ and Nu. The heat transfer at this location appears to be governed by the directly impinging channel flow. At Y = 1, both θ and Nu increase evenly with each

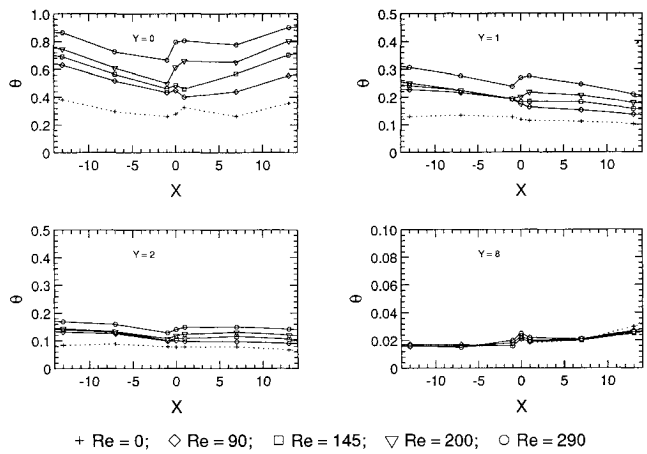

Fig. 6 Effect of Reynolds number on the temperature distribution in the perpendicular gap (T_c = 10°C; H_s = 0).

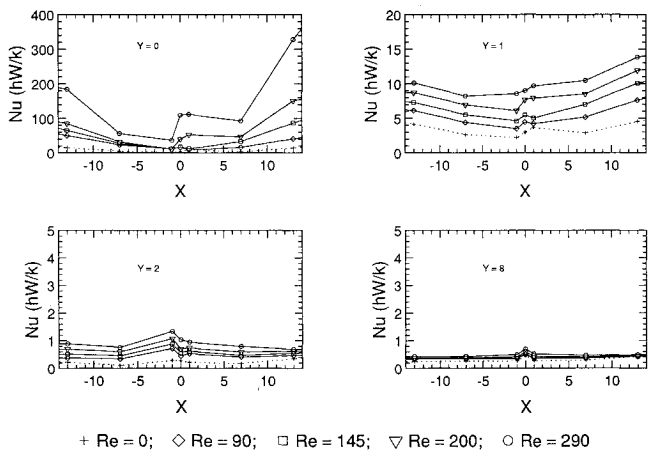

Fig. 7 Effect of Reynolds number on Nusselt numbers in the perpendicular gap (T_c = 10°C; H_s = 0).

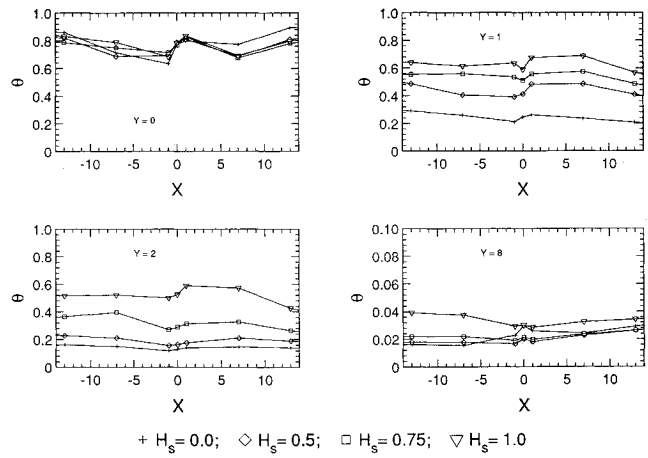

Fig. 8 Effect of step height on the temperature distribution in the perpendicular gap (T_c = 5°C; Re = 290).

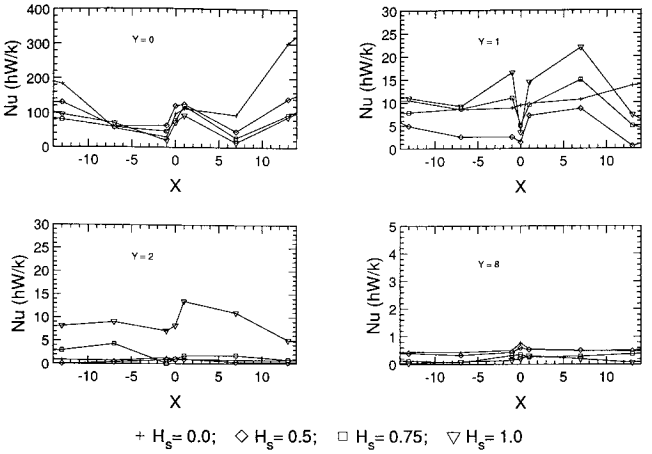

Fig. 9 Effect of step height on Nusselt numbers in the perpendicular gap (T_c = 5°C; Re = 290).

increment in H_s ($=h_s/W$). Deeper into the groove, significant increases in θ and Nu are realized for the larger step heights of 0.75 and 1.0. The increase in H_s causes a corresponding increase in penetration into the gaps, and increasing rates of convection. Thus, tile-height differences primarily alter the thermal stratification within the perpendicular gap; asymmetries in θ and Nu around the centerline are largely unaffected.

At a depth of $Y = 8$, however, the temperatures and convection rates again become independent of the step height. Thus, it appears that for step heights of $H_s > 0.5$, the region of direct penetration of channel flow extends below $Y = 2$. The actual depth of penetration must lie in the range $2 < Y < 8$. This increase in penetration depth with increasing step height is in agreement with the flow visualization results discussed earlier.

Natural Convection Heat Transfer

Natural convection and conduction were found to be the predominant modes of heat transfer in the perpendicular gap, but for the extent of a few gap widths at the top where forced convection plays a role. To further study natural convection in the gap, a test case was chosen with no flow ($Re = 0$), at a coolant temperature of 10°C. Temperatures (θ) at zero flow are included in Fig. 6 as a function of X ($Re = 0$). This enables a comparison of the forced convection results with the no-flow, natural convection situation. Results are presented at $Y = 0$, 1, 2, and 8; different Y scales were needed to properly represent the data. Corresponding Nusselt numbers at zero flow are included in Fig. 7.

The temperature profiles are strongly dependent on Re for $Y = 0$, 1, and 2, as discussed earlier. In addition, it is clear that zero-flow temperatures in natural convection lie well below those with finite channel flow rates. At $Y = 8$, however, there is little change in θ for any Re, including $Re = 0$. An interesting feature of Fig. 6 is that even with no flow, the temperatures are not independent of X, especially at $Y = 0$ (the top surface). The temperatures are lower near the centerline and increase with distance from the centerline. At $Y = 1$, 2 and 8, the temperatures are fairly uniform across X (note that fluctuations in the profiles at $Y = 8$ are on a much smaller scale than the other graphs). The reasons for the depression in centerline temperatures for $Y = 0$ appear to be twofold: 1) the presence of one end of the cold parallel gap heat exchanger on the opposite wall; and 2) the presence of the parallel gap itself allows for larger convection currents to be set up near the centerline, while the rest of the perpendicular gap is constrained by two walls. These convection currents bring cooler fluid from lower down in the gaps up to the surface, near the centerline of the perpendicular gap, causing the lower temperatures observed at $Y = 0$.

Just as for the temperature profiles, Nusselt numbers also increase significantly as Re increases from 0 in the region $Y \leq 2$, and are independent of Re at $Y = 8$, as shown in Fig. 7. Fluctuations in the Nu profiles near the centerline even for $Re = 0$ are similar to those found in the temperatures of Fig. 6. Treating the perpendicular gap heat exchanger as a vertical plate in an infinite quiescent medium, the natural convection Nusselt number would be 48 (at the top, $Y = 0$). The experimental value on the other hand is approximately 8 at this location. The finite gap width therefore decreases Nu within the gap by a factor of 6. Nusselt numbers over most of the gap, however, are close to unity, indicating a conduction/asymptotic regime of natural convection (MacGregor and Emery[11]).

Conclusions

The flow and convective heat transfer patterns obtained in this study are largely a result of the very narrow nature of the gaps (depth/width = 20). Penetration of external flow into the perpendicular gap was thus limited in most cases to roughly two gap widths while greater entrainment occurred in the parallel gap. Secondary flows in the perpendicular gap arose from fluid entrained in the parallel gap and projected towards the obtuse ($+X$) side. This led to asymmetries about the centerline in the perpendicular gap flow patterns, temperatures, and convection coefficients. Natural convection was the predominant mode of heat transfer in the bulk of the perpendicular gap, especially at depths of over 8 gap widths.

Of the system parameters varied, Reynolds number and relative tile-height differences had the strongest influence on heat transfer. This influence was, however, limited to the primary-vortex region, i.e., to a depth of 1–2 gap widths. These changes in the system parameters affected both the magnitude and the asymmetry of the temperature and flowfields. An increase in Reynolds number from 90 to 290, or in the height of the perpendicular tile by one gap width, caused the penetration depth to increase to 2–3 gap widths from between 1–2. Variation in coolant temperature had a negligible effect on heat transfer coefficient.

The insight gained from the present study into the flow patterns and heat transfer at intersections in tile gaps should be applicable towards developing more realistic numerical models.

Acknowledgment

Support for this work through the NASA Ames Consortium Agreement NCA 2-451 is gratefully acknowledged.

References

[1]Scott, K. D., and Mariah, R. J., "Gap Heating with Pressure Gradients," *Entry Heating and Thermal Protection*, Vol. 69, Progress in Astronautics and Aeronautics, AIAA, New York, 1979, pp. 269–286.

[2]Dwoyer, D. L., Newman, P. A., Thames, F. C., and Melson, N. D., "A Tile-Gap Flow Model for Use in Aerodynamic Loads Assessment of Space Shuttle Thermal Protection Systems: Parallel Gap Faces," NASA TM 83151, Oct. 1981.

[3]Neary, M. D., and Stephanoff, K. D., "Shear-Layer-Driven Transition in a Rectangular Cavity," *Physics of Fluids*, Vol. 30, 1987, pp. 2936–2946.

[4]Pan, F., and Acrivos, A., "Steady Flows in Rectangular Cavities," *Journal of Fluid Mechanics*, Vol. 28, Pt. 4, 1967, pp. 643–655.

[5]Rhee, H. S., Koseff, J. R., and Street, R. L., "Flow Visualization of a Recirculating Flow by Rheoscopic Liquid and Liquid Crystal Techniques," *Experiments in Fluids*, Vol. 2, 1984, pp. 57–64.

[6]Koseff, J. R., and Street, R. L., "The Lid-Driven Cavity Flow: A Synthesis of Qualitative and Quantitative Observations," *Journal of Fluids Engineering*, Vol. 106, 1984, pp. 390–398.

[7]Jaroch, M. P., and Fernholz, H.-H., "The Three-Dimensional Character of a Nominally Two-Dimensional Separated Turbulent Shear Flow," *Journal of Fluid Mechanics*, Vol. 205, 1989, pp. 523–552.

[8]Garimella, S. V., and Eibeck, P. A., "Heat Transfer Characteristics of an Array of Protruding Elements in Single Phase Forced Convection," *International Journal of Heat and Mass Transfer*, Vol. 33, No. 12, 1990, pp. 2659–2669.

[9]Koseff, J. R., and Street, R. L., "On End Wall Effects in a Lid-Driven Cavity Flow," *Journal of Fluids Engineering*, Vol. 106, 1984, pp. 385–390.

[10]Shollenberger, K. A., "Flow Within Tile Gaps on Space Vehicles: A Heat Transfer and Flow Visualization Study," Masters' Project Rept., Univ. of California at Berkeley, Berkeley, CA, 1991.

[11]MacGregor, R. K., and Emery, A. P., "Free Convection Through Vertical Plane Layers: Moderate and High Prandtl Number Fluids," *Journal of Heat Transfer*, Vol. 91, 1969, pp. 391–403.